PCCP

Accepted Manuscript

This is an *Accepted Manuscript*, which has been through the Royal Society of Chemistry peer review process and has been accepted for publication.

Accepted Manuscripts are published online shortly after acceptance, before technical editing, formatting and proof reading. Using this free service, authors can make their results available to the community, in citable form, before we publish the edited article. We will replace this *Accepted Manuscript* with the edited and formatted *Advance Article* as soon as it is available.

You can find more information about *Accepted Manuscripts* in the **Information for Authors**.

Please note that technical editing may introduce minor changes to the text and/or graphics, which may alter content. The journal's standard **Terms & Conditions** and the **Ethical guidelines** still apply. In no event shall the Royal Society of Chemistry be held responsible for any errors or omissions in this *Accepted Manuscript* or any consequences arising from the use of any information it contains.

Strain Engineering the Properties of Graphene and Other Two-Dimensional Crystals

Mark A. Bissett*[‡], Masaharu Tsuji and Hiroki Ago*

Institute for Materials Chemistry and Engineering, Kyushu University, Fukuoka, 816-8580, Japan.

E-mail: ma-bissett@cm.kyushu-u.ac.jp, ago@cm.kyushu-u.ac.jp

Abstract

Graphene has been widely studied for its many extraordinary properties, and other two-dimensional layered materials are now gaining increased interest. These excellent properties make thin layer materials very attractive for integration into a wide variety of technologies, particularly in flexible optoelectronic devices. Therefore, gaining control over these properties will allow for a more focused design and optimisation of these possible technologies. Through the application of mechanical strain it is possible to alter the electronic structures of two-dimensional crystals, such as graphene and transition metal dichalcogenides (e.g. MoS_2), and these changes in electronic structure can alter their behaviour. In this perspective we discuss recent advances in the strain engineering of thin layer materials, with a focus on using Raman spectroscopy and electrical transport to investigate the effect of strain as well as the effect of strain on the chemical functionalisation of graphene.

Introduction

Graphene, a single-atom thick sheet of hexagonal sp^2 hybridised carbon atoms, has been the focus of an immense amount of research in recent years due to its many extraordinary properties. These properties include exceptionally high charge carrier mobility,[1,2] high mechanical strength and elasticity,[3,4] optical transparency,[5,6] and a wide variety of possible chemical modifications.[7-9] Each of these attributes makes graphene an ideal material to investigate not only fundamental scientific questions regarding condensed matter physics, but also practical integration into a wide variety of devices including flexible electronics,[10-13] photonic devices,[14,15] and transistors.[16,17] However, despite these excellent properties

graphene still faces several drawbacks, including the lack of a band gap due to the contact between the conduction and valence bands at the Dirac points (*K* point), as well as difficulty in scaling up production while maintaining high quality. The beneficial properties of graphene can be modified or tuned for specific applications, and other unique properties introduced, by a variety of methods; including confining the size into zero-dimensional (0D, quantum dots) or one-dimensional (1D, ribbons) structures,[18,19] altering the number of graphene layers,[20,21] chemical functionalisation,[22-24] as well as applying mechanical strain.[25-28]

The effects of mechanical strain on graphene are important to understand, particularly for applications such as flexible electronics. Strain allows the electronic structure of graphene to be easily altered, and also the possibility of introducing a band gap into the otherwise gapless material.[25,28-30] However, it has been calculated that strain values over 20% are needed to open a significant band gap in graphene,[29-31] although this value depends strongly on the relative angle of applied strain. Typical experimentally realised strain values are much lower, approximately 1%, far below the predicted maximum for graphene. However, strain values as high as 30% have been reported using suspended graphene[4] and this indicates that, in principle, much higher strain values are possible. The much lower strain values typically achieved are the result of poor strain transfer between graphene and its supporting substrate.[32-34] The majority of existing publications pertain to theoretical calculations on how the distortion of the graphene lattice can lead to changes in the electronic structure and how this can affect the properties of graphene. In the theoretical studies typically the strain studied is homogenously distributed across the sample by uniaxial or biaxial tension and compression. However, some studies have shown that non-uniform strain can lead to unique electronic and photonic properties in 2D crystals;[26,35] however the experimental realisation of such complex strain is still difficult to achieve. Experimentally strain can be applied by either bending or stretching the supporting substrate to induce strain. The strain induced in the graphene experimentally is therefore a combination of in-plane tension/compression as well as shear strain due to substrate interactions. Out-of-plane strain, perpendicular to the graphene, can also be

induced due to buckling and the formation of ripples. As mechanical strain is applied to the graphene, the lattice becomes distorted and the Dirac cones are shifted at the *K* and *K'* points in opposite directions, leading to a modulation of the electronic structure.[27] As well as shifting the Dirac cones, mechanical strain causes a change in the Fermi velocity in graphene.[27,36] Depending on the strain axis, either along the armchair or zig-zag directions, the Fermi velocity typically decreases for tension, while increasing for compression.[36] These changes to the electronic structure will alter the behaviour of strained graphene, particularly in electronic devices. As mechanical strain alters the separation of the Dirac cones, as well as the dispersion within each cone, these changes can be easily detected by Raman spectroscopy, and there are a large number of existing works that investigate the Raman spectra of strained graphene.

Chemical functionalisation of graphene is of interest due to the ease of up-scaling for wide scale production and the reactivity of graphene, as well as other 2D materials, can be modified by applying strain. Functionalisation of graphene is of interest as it can modify the electronic structure through doping,[37] allowing for the synthesis of p- and n-doped graphene *via* the attachment of electron withdrawing and donating molecules respectively.[38,39] Due to the stability of graphene's sp^2 carbon network it is typically considered chemically inert. Fullerenes and carbon nanotubes are known to have high chemical reactivity due to the strain present in their highly curved lattice,[40-42] which causes them to release this strain through the formation of sp^3 covalent attachment sites. The source of graphene's chemical stability comes, in part, from the reduced strain present in its sp^2 network due to its ideal planar structure. However, despite graphene's low reactivity several synthetic routes have been demonstrated to be particularly effective including; the use of highly reactive radicals, nucleophilic addition, cyclo addition, and electrophilic substitution.[43-45] By applying strain to the graphene lattice one can engineer its chemical reactivity and this in turn can greatly alter its properties allowing the tuning of the electronic structure as needed.

As mentioned, due to the flexibility, optical transparency, and high carrier mobility of graphene applications such as flexible electronics are made possible. To investigate the performance of flexible

graphene electronics, the effect of strain on the electrical transport properties of graphene is required. Conventional materials such as silicon are unacceptable for integration into flexible devices due to poor flexibility and transparency, while organic semiconductors suffer from low carrier mobility. However, the combination of graphene and flexible supporting substrates may allow for these drawbacks to be overcome.[46] Flexible graphene based transistors have been produced that can operate in a range of applied strains.[10-13] Typically, as graphene is strained the resistance increases and the carrier mobility decreases, however this can also be utilised in the form of highly sensitive strain sensors.[47-51] To fully optimise the performance of the flexible graphene based electronics it is essential to fully understand the effect of strain on the electrical properties.

As well as graphene, other two-dimensional (2D) layered materials are also of interest due to their unique properties, many of which are also affected by both strain and chemical functionalisation. In particular inorganic materials such as transition metal dichalcogenides (TMDs)[52] are gaining increased research focus, due to similarities with graphene. TMDs have the advantage of being intrinsic semiconductors, expanding the possibilities for applications in electronic and optoelectronic devices. Also, some TMDs show unique layer-number dependant electronic band structures, changing from indirect to direct gap with decreasing layer number. Already there are several examples of similar effects of mechanical strain on such materials including increased catalytic activity[53] and altering of their electronic structure,[35,54-57] as well as the effect of curvature on chemical activity.[58] There are also many combinations of graphene and other 2D materials that can be combined into heterostructures,[59,60] which when combined with strain engineering will allow novel properties and applications to be explored.

In this Perspective we provide an overview of strain engineering of 2D layered materials, with particular focus on the use of Raman spectroscopy, chemical functionalisation and electrical transport of strained graphene. As well as graphene, we also briefly discuss related 2D layered materials, such as MoS_2, which exhibit similar behaviour. We highlight recent results, both theoretical and experimental, as well as discussion of future directions of this field.

1. Raman Spectroscopy of Strained Graphene

Raman spectroscopy is an ideal method to investigate the properties of graphene as it provides a wealth of information regarding the physical and electronic structure while being fast and non-destructive.[61,62] Raman spectroscopy allows one to determine the number of layers of graphene present in a sample,[63,64] detect the presence and concentration of defects,[65,66] determine the level and polarity of doping,[67-70] as well as the effect of strain on the graphene lattice.[71-73] As mentioned previously, mechanical strain can alter the electronic structure of graphene by distorting the graphene lattice. This lattice distortion can be easily detected by Raman spectroscopy. As mechanical strain is applied to the graphene there are several key changes that occur to the Raman spectrum, in particular tensile strain causes an increase in Dirac cone separation leading to phonon softening (red shift of the signature graphene Raman peaks) while compressive strain leads to phonon hardening (blue shift).[71,74] The shift in peak position (ω) with applied strain (ε) is linear; this allows one to use Raman spectroscopy to determine the level of strain on the graphene from the Raman shift.[27,75,76] However, this typically requires assumptions regarding the homogeneity of the applied strain as well as treating the strain as purely uniaxial or biaxial. In reality most experimental apparatuses apply a combination of strain along several different axes making the interpretation of the data more complex. Applied strain also leads to the splitting of the doubly degenerate G band into separate peaks, referred to as the G^+ and G^-, while the 2D (or G´) band also splits under applied strain into separate $2D^+$ and $2D^-$ peaks.[71,72] Thus, by measuring the Raman spectrum of graphene that is undergoing externally applied strain it is possible to gather a wealth of information about the phonon structure and use strain to tune the properties of graphene as required.

Several groups have investigated the effect of strain on graphene by Raman spectroscopy and this peak splitting and subsequent shift in phonon frequency of the G band are demonstrated in Fig. 1. Figure 1a depicts the G band of relaxed (grey) and strained graphene (black), demonstrating how the peak splits into two separate peaks (referred to as the G^+ and G^-), due to the angle between the applied strain axis and

the orientation of the graphene lattice.[77] As the degree of peak separation depends strongly on the relative angle between the lattice and the strain axis, it is possible using polarized Raman to determine the orientation of the graphene lattice while strain is applied.[78] This can be used to generate a map showing the different domain orientations in polycrystalline graphene. Figure 1b plots the position of each of the G band sub peaks (G^+, G^-) as a function of applied strain up to 1%, demonstrating the linear dependence. The slope of this relationship ($\partial\omega_G/\partial\varepsilon$, where ω_G is the frequency of the G and ε the strain) is inherent to the material, but changes for uniaxial *versus* biaxial strain, and several different values are reported for single-layer graphene in the literature depending on the method of calculation or experimental setup.[71,73,74] Typical values of $\partial\omega_G/\partial\varepsilon$ for uniaxial strain of the G^- and G^+ are 33 cm^{-1}/% and 15 cm^{-1}/%, respectively.[74] This linear dependence of peak position on Raman shift allows for sensitive strain sensors to be designed on graphene containing fibres or similar nanocomposites.[77] Through the addition of polarised Raman it would also be possible to determine not only the magnitude of strain but also the orientation of the strain axis, an important tool for investigating the mechanical properties of nanocomposite materials. Figure 1c shows the Raman spectra of graphene undergoing a range of strain values from tension into compression, as is standard in the literature, tension is depicted as positive strain values (up to 0.62% in Fig. 1c) while compression is given as negative strain (down to -0.62%).[79] We can clearly see in Fig. 1c that as tension is applied the G band phonon frequency softens (downshifts) in frequency and begins to split into two discrete peaks, while compression causes phonon hardening or upshifting in frequency combined with the similar splitting.

The 2D peak also undergoes splitting when strain is applied, as shown in Fig. 2.[72,80] Figure 2a shows the Raman spectra of graphene with increasing strain when the excitation light is polarised parallel (red) or perpendicular (black) to the strain axis. The 2D band, even without applied strain, in made up of two Lorentzian components, then as strain is applied these shift at differing rates.[81,82] This is because unlike the single photon G band Raman process, the 2D band is a double resonance process involving two phonons.[62] Due to this two phonon process when strain is applied the distorted lattice allows for new

resonant conditions to apply, thus the 2D band is affected not only by phonon softening due to strain but additional shift due to a shift in the Dirac cones.[72,82,83] The linear response of the 2D peak positions with applied strain can be seen in Fig. 2b. The sensitivity of the 2D band to strain ($\partial\omega_{2D}/\partial\varepsilon$) is approximately double that of the G band, with typical values of 63.1 cm^{-1}/% and 44.1 cm^{-1}/% for the 2D$^-$ and 2D$^+$ peaks respectively for uniaxial strain applied along armchair direction.[80] Figure 2c illustrates the spectrum of strained graphene for differing angles of plane polarised excitation, demonstrating that the 2D$^+$ and 2D$^-$ are at maximum intensity perpendicular to one another. This is because they originate from differing axis in the graphene lattice, and can be represented on a polar plot with separate lobes for each sub-peak.[80]

Typically experiments into the effect of strain on graphene have used mechanically exfoliated samples that are transferred onto a flexible polymer substrate and then bent using a cantilever apparatus. Recently, we have experimentally investigated the effect of shear strain (in-plane distortion) on the Raman spectrum of both pristine[76] and chemically functionalised[84] chemical vapour deposition (CVD) grown graphene. Typically strain occurs as either uniaxial compression or tension however, due to the interactions between the supporting substrate and the graphene shear strain can become the dominant mechanism, which is as a combination of tension and compression perpendicular to each other. This inhomogeneous biaxial strain has been investigated theoretically previously and is of interest as it can more greatly affect the electronic structure of graphene than uniaxial strain alone.[29,85] Although CVD growth can produce large-area single-layer graphene with relatively low cost the as-grown graphene usually contains many small domains with differing orientations, with the interface between these rotated domains containing defect rich domain boundaries,[86,87] due to the uncontrolled formation of nucleation sites and un-optimised growth conditions. The use of CVD grown graphene results in a polycrystalline structure with many domain boundaries. These domain boundaries are an important feature, as they affect not only the mechanical properties of the graphene[88-91] but also the electronic structure.[92,93] Despite the generally assumed negative side-effects of domain boundaries, there are in fact a wide variety of novel

properties and applications that are made possible by domain boundaries, including plasmonics[94] and electronics.[95]

These domain boundaries consist of a wide variety of defective structures, but predominantly chains of pentagon-heptagon rings (5-7), such a structure can be seen in Figs. 3a and 3b, along with theoretical models of polycrystalline graphene, in Figs. 3c and 3d. Figure 3a shows an atomic resolution annular dark-field scanning transmission electron microscope (ADF-STEM) image of CVD grown graphene containing a domain boundary, with Fig. 3b showing the same boundary with the 5-7 ring defects highlighted.[86] The domains on either side of the boundary are measured to be rotated by 27° to each other, and it is this mismatch that causes the defective boundary to form at the interface. Figure 3c is a theoretical model of polycrystalline graphene showing several domains with different rotations.[96] These domain boundaries cause the graphene to not exist as an ideal flat sheet, but instead an uneven and undulating surface due to inherent strain on the surrounding lattice. These imperfections in the graphene surface are important to take account of when predicting the properties and behaviour of polycrystalline graphene. As mechanical strain is applied to the polycrystalline graphene lattice, it is not dispersed homogenously across the lattice. Instead defects, such as those present along domain boundaries, undergo significantly increased strain,[90,96,97] a similar effect has also been calculated for carbon nanotubes.[98] This is shown in Fig. 3d, where a line of alternating 5-7 member rings is shown to induce significant stress along the boundary compared to the inner domain regions.[97] This pre-strain existing in the lattice due to the 5-7 ring defects causes them to undergo increased deformation when external strain is applied.

Strain can also induce other mechanisms, such as domain rotation or slippage due to inefficient interfacial strain transfer. The relative orientation of the boundary with respect to the applied strain is also an important factor.[99,100] However, in the case of CVD graphene the orientation of these domain boundaries is typically random so there is little control of such relative orientation. Recently, we found that the use of polycrystalline graphene, containing domains ranging in size from several hundred nanometres to over one micron, led to an unexpected trend in the Raman peak positions with increasing

mechanical strain.[76] As mechanical strain is applied to the polycrystalline graphene the domain boundaries undergo increased strain due to their already strained defective structures.[90,97,101] The presence of this strained defective lattice then causes the phonon frequencies to be affected. Shown in Fig. 4a is the typical shift of the G and 2D bands for exfoliated graphene, with a negative slope ($\partial\omega/\partial\varepsilon$) as expected. However, when polycrystalline graphene was transferred onto polydimethylsiloxane (PDMS) and shear strain was applied, as shown in the diagram of Fig. 4b, the G and 2D bands were observed to have opposite slopes. As PDMS was used as the flexible substrate and the supporting substrate was elongated, the graphene underwent compression producing an upshift of the 2D band position as expected, however the G band was found to decrease in frequency. This unexpected behaviour was attributed to the presence of domain boundaries, due to the absence of such behaviour in exfoliated or CVD grown large (>100 μm) domain graphene which both behaved as expected. These results suggest that only when the graphene domain size is smaller than the Raman laser spot size (approximately 1μm) would this opposite trend in peak position be observed. The reason behind this opposite trend in phonon frequency for the G and 2D bands is likely related to the physical origins of each band. The G band originates from a first order single phonon process, while the 2D band originates from a second-order process where two iTO phonons scatter near the K point.[62] The 2D band originates independently from defects within the graphene structure and thus is a measure of the strain within the domain areas. While the G band is more strongly affected by both strain within the domain and along the boundary and contains information regarding the changing force constant as strain is applied.[76] The differing phonon scattering processes will affect how each Raman peak behaves as strain is applied to the already strained domain boundaries. The behaviour of strained domain boundaries may lead to unexpected physical or electrical properties that can be exploited, making understanding the effect of strain on polycrystalline graphene of great importance.

2. Chemical Reactivity of Strained Graphene

One application that arises from the alteration of the electronic structure of graphene as mechanical strain is applied is enhanced chemical reactivity. As discussed previously the reactivity of carbon sp^2 systems depends strongly on the internal strain that results from curvature within these systems. This curvature is best described by π-orbital axis vector (POAV) theory,[41,42] which describes how the relative angle between the π-orbital and the σ-orbital is related to the chemical reactivity of the carbon atoms. Thus, fullerenes[42] and carbon nanotubes[40] have a high intrinsic reactivity due to the curvature of their surfaces, on the other hand pure 2D materials such as graphene have very low reactivity. The low reactivity of graphene typically requires harsh chemical treatment to allow functionalisation to occur. However, as we have seen it is also possible to distort the lattice of graphene by applying mechanical strain, and this would be expected to have an effect on the chemical reactivity of the graphene allowing for control over the subsequent properties. There have been several theoretical investigations into the effect of mechanical strain on the chemical reactivity of graphene, but only recently have these been experimentally achieved. Defect sites, including point defects, edges and domain boundaries, in graphene have also been both theoretically predicted and experimentally observed to have increased chemical reactivity.[84,102-105] Therefore we would expect the combined effect of mechanical strain on defect rich structures to be of interest for controlling the chemistry of graphene.

Theoretical calculations have shown that as graphene is strained the charges around each of the carbon-carbon bonds becomes localised. This charge localisation can lead to increased binding energy for simple molecules such as hydrogen[106-108] and also enhanced adsorption of metal nanoparticles.[109,110] There have also been some studies on the covalent functionalisation of graphene, comparing the different effect of strain on physisorption and chemisorption.[111,112] The increased binding energy of hydrogen on strained graphene was first published in 2008, and calculated that the binding energy depended linearly on applied strain.[106] Applied tensile strain was calculated to weaken the π-bond, creating an extended p_z-like orbital

that is able to form a covalent bond, that with approximately 10% strain could increase the reactivity of the graphene by a factor of 5.[106] This elongation of the C-C bonds and subsequent localisation of the π electrons can be seen in Fig. 5a. It has been calculated that as graphene undergoes biaxial strain the increased charge density also leads to the formation of new peaks in the density of states (DOS), and these new peaks shift towards the Fermi level.[108] Calculations for other simple atoms and molecules such as a single atom of hydrogen, fluorine, or oxygen, and a hydroxyl group have been performed.[111]

Figure 5b plots the change in energy of pristine graphene with applied strain along both the zig-zag and armchair directions as well as biaxial strain.[111] It can be clearly seen that as strain, either compression or tension, is applied to the graphene that the total energy increases. The uniaxial strain applied along both the armchair and zig-zag directions produces an approximately equal increase in energy, however biaxial strain destabilises the graphene more significantly leading to increased total energy. This increased energy from destabilisation of the graphene lattice can decrease the chemisorption energy for all studied adatoms.[111] It was also discovered that large negative strain, or compression, leads to the formation of ripples in the topology of the graphene and this localised curvature can also affect the reactivity of the graphene. The formation of ripples in the topology of graphene has also been calculated to occur for shear strain as seen in Fig. 5c.[113] Thus we can expect the increased chemical reactivity from strained graphene to be a combination of charge localisation and also the formation of localised curvature through the formation of ripples and other topological defects.

Calculations have also been performed for metal clusters in contact with strained graphene, in particular platinum clusters were proposed to possess increased binding energy as well as controllable catalytic activity based on *ab initio* calculations.[109] The correlation between applied strain (%) and binding energy of platinum (E_b^{Pt}) can be seen in Fig. 5d. It was found that as biaxial strain is increased the binding energy towards the platinum cluster increases linearly. The reason for the increased binding energy was given as increased electrostatic potential at the platinum/graphene interface,[109] itself a result of increased charge density in the strained graphene as already discussed. The catalytic properties of the

platinum nanoparticles were also affected by the strain on the underlying graphene supporting substrate, due to alterations of the DOS of the platinum cluster as strain was applied to the graphene.[109] It was also found that strained graphene suppresses the degradation of the catalyst clusters providing a more durable system. This is an example of how strained graphene can be used to dynamically tune the properties of catalyst particles for specific requirements.

In addition to the existing theoretical calculations already published there have been experimental confirmations of the increased reactivity of strained graphene systems. One recent publication demonstrated that strain on graphene induced by localised curvature can lead to increased reactivity towards diazonium functionalisation.[114] Aryl diazonium functionalisation is particularly interesting due to the well-established reactivity with sp^2 carbon systems and the ability to tune the electronic properties of the graphene through doping.[9,24,39,115] The mechanism by which aryl diazonium molecules attach is via an initial electron transfer step that forms a highly reactive aryl radical, this radical then rapidly covalently attaches to the graphene converting the lattice at the attachment site from sp^2 to sp^3 hybridisation.[44,45] The increased reaction with aryl diazonium, 4-nitrobenzene diazonium (4-NBD) was achieved by deformation of the graphene by transferring it onto spherical silica (SiO_2) nanoparticles, creating ripples in the graphene, and then chemically functionalising the graphene as shown in Fig. 6a. It was observed that by transferring the graphene onto these silica nanoparticles that the curvature induced strain gave rise to an increased rate of reactivity, detected as a larger change in the Raman spectrum of the graphene.[114] Figure 6b shows the Raman map plotting the D band intensity of the deformed graphene before (1) and after (2) diazonium functionalisation. At locations of increased deformation there is a corresponding amount of increased functionalisation, this increased degree of covalent functionalisation was attributed to curvature induced strain and can be determined by the increased intensity of the D band in the Raman spectrum in Fig. 6c, indicative of covalent attachment. These results were also supported by theoretical calculations which showed that by increasing the curvature of the graphene the pyramidalization angle was increased, leading to increased reactivity.[114]

Strain can also be applied to graphene in a dynamic fashion allowing for a tuning of the chemical reactivity to be achieved. Recently, we demonstrated that graphene transferred onto a flexible supporting substrate (PDMS) can be functionalised while external mechanical strain was applied; this is shown schematically in Fig. 7a.[116] Several different aryl diazonium molecules were used; either p-type dopants (nitrobenzene, bromobenzene) or n-type dopants (methoxybenzene) and increased reactivity was observed for each species. It was observed that applying strain of up to 15% to the supporting substrate resulted in an increase in the rate of functionalisation up to 10 fold.[116] The saturation concentration of attached molecules was also found to increase with applied strain, possibly allowing for sufficient yield to open a significant band gap in the electronic structure of the graphene. The increased functionalisation was confirmed by both an increase in the I_D/I_G ratio due to covalent bond formation, a decrease in the I_{2D}/I_G ratio due to charge transfer, as well as increased peak shift due to doping.[116] The origin of this increased reactivity was attributed to the increased charge localisation as previously predicted theoretically. As aryl diazonium reactions require an electron charge transfer step to initiate it is reasonable to see how increased electron density around the carbon atoms leads to increased covalent functionalisation occurring. For the n-type dopant, methoxybenzene compound (4-MBD), the rate of functionalisation on relaxed graphene was found to be negligible, but with 15% applied strain both the rate and the degree of doping and functionalisation was found to increase drastically, as can be seen in the plot of the I_D/I_G ratio and Raman spectra of Fig. 7b,c. This increased reactivity of graphene under mechanical strain can allow for reactions to take place that would not be possible for relaxed graphene. In this way the strain can act as a reversible 'catalyst', possibly allowing a wider variety of reactions to take place and expanding the possibilities for the chemical functionalisation of graphene. The use of this strain enhanced reactivity can allow for sufficient doping to be achieved making it suitable for electronics applications, for example by functionalising opposing areas of graphene with p- and n-type dopants an in-plane p-n junction can be created.[116] This is one example of tuning the properties of graphene for flexible electronics applications. Theoretical DFT calculations were also used to support the increased chemical reactivity observed experimentally. In particular it was calculated that strain applied to defect containing

graphene undergoes significant destabilisation, leading to an increase in total energy, while pristine graphene is not strongly affected.[116]

3. Flexible Graphene Electronics

For applications in the electronic industry the charge transport properties of graphene while undergoing strain are of importance. As discussed in the previous sections, as graphene is strained to sufficiently high values the electronic structure can be altered and this changes the charge carrier transport through the graphene. This is particularly important for the design of flexible electronic devices, such as field-effect transistors (FETs) and transparent electrodes.[10-13] These previous devices have demonstrated that graphene transferred onto flexible and stretchable substrates are a viable technology, however, they still suffer from several drawbacks. Firstly, as the graphene is brought into contact with the supporting polymer substrate the desired exceptional carrier mobility is often severely reduced due to scattering and thus several layers of graphene are needed to overcome this. The use of multiple graphene layers reduces the contact resistance of the device and removes the need for metal contacts which typically deteriorate under large strain. Secondly, current experimental devices operate at much lower strain regimes than has been theoretically predicted to be required to significantly alter the band structure of graphene. However, a transport gap can be introduced into areas of highly localised strain which leads to suppressed conductivity even in the absence of a bulk band gap.[25,31] Understanding the performance of flexible graphene devices while undergoing strain is important to enable future developments and optimise device design and construction.

Figure 8 demonstrates the construction and electrical characterisation of a flexible graphene based FET.[13] In Fig. 8a we can see a schematic showing the patterned graphene (1-3 layers) supported by a flexible PDMS substrate as well as a printed ion gel gate. Figure 8b shows the charge transfer characteristics for increasing thickness of graphene displaying ambipolar behaviour, while Fig. 8c shows the charge carrier mobility as a function of graphene thickness. With only one graphene layer the charge

scattering caused by substrate interactions greatly reduces the mobility, and as the number of graphene layers increases so does the mobility with 3 layers showing greatly improved performance while retaining optical transparency.[13] Figure 8d shows the optical images as the FET is strained, as determined by the change in length of the PDMS, up to 5%. However, due to inefficient strain propagation between layers it is likely that the top-most layer is experiencing significantly reduced strain, as discussed in the earlier section.[117] Figure 8e shows the I-V curve behaviour of the tri-layer graphene FET with increasing strain up to 5%, which showed only a minor decrease in performance corresponding to a 15% drop in mobility. Above 5% strain the decrease in performance was more severe (Fig. 8f), attributed to the formation of cracks in the graphene film. Below this 5% threshold the device was highly reproducible, showing little degradation after 1000 cycles of strain/release of 3%. This example demonstrates that graphene can be used to effectively design and construct flexible electronic devices that function even while being bent and stretched. The performance of such flexible graphene based transistors can be further improved by better understanding the interaction between the polymer substrate and the graphene layer in terms of interfacial strain transfer and charge scattering. This may allow such devices to operate in much higher strain regimes that can then more significantly alter the electronic structure of the graphene as theoretically predicted. By choosing appropriate materials and synthesis conditions it may be possible to create highly durable and resilient flexible, transparent electronic devices.

Another possible application of graphene that is transferred onto flexible supporting substrates is highly sensitive strain sensors or strain gauges. These gauges work on the principle that mechanical strain will increase the resistance of the graphene, and that very small strain can be easily detected and quantified. The sensitivity of a strain gauge, known as the gauge factor, is defined as the change in relative resistance as a function of applied strain ($\partial(\Delta R/R_0)/\partial\varepsilon$) and is typically linear. The linear change in the relative resistance with applied strain has been attributed to the relative change of the Fermi velocity under strain. By calculating the slope of the Dirac cones from DFT calculations the relative Fermi velocity can be determined and related to the gauge factor.[50] By theoretically calculating the gauge

factor of suspended graphene using the Fermi velocity it was found to be 2.4 while the experimental value determined from resistivity was 1.9, in good agreement with one another.[50] It was suggested that the increase in resistivity with strain could be attributed to the increase in carbon-carbon bonds, similar to conventional metallic materials.[47] Several strain sensors have been reported for graphene on flexible polymer substrates, however due to the differences in methods of graphene synthesis, transfer, and choice of polymer substrate the gauge factor values cover a wide range; such as ≈2,[49,50] 4-14,[47] 6.1,[51] 22,[48] or 151.[118] In these previously published results single-domain exfoliated graphene is found to have the lowest sensitivity to strain[49,50] while the existence of grain boundaries in CVD grown polycrystalline graphene make it much more sensitive at lower strain regimes.[48,118]

The possibility of such high sensitivity allows these graphene based strain gauges to operate as tactile sensors that could be integrated into clothing or used for other forms of feedback. Figure 9 shows an example of one such graphene based strain sensor.[47] Due to the reduced mobility of single-layer graphene in contact with flexible substrates, as previously discussed, the device shown in Fig. 9a consists of approximately 10 layers of graphene supported by PDMS and patterned into a rosette to maximise strain sensitivity. Typically single layer graphene devices require metal contacts be deposited to allow for electrical measurements due to the high contact resistance arising from the small contact area, however by increasing the number of graphene layers the contact resistance is greatly reduced, removing the need for metal contacts to be attached to the device; instead electrodes can be directly contacted onto the graphene stack. Figure 9b is a plot of the resistance as a function of applied strain (measured by the change in substrate length) showing that resistance increases with increasing strain. As with the previous example, at lower strain regimes (<5%) the device response to strain was found to be highly reproducible, however at higher strains (>5%) the performance was found to be non-reproducible and the original performance could not be recovered.[47] The gauge factor of the device in Fig. 9b was calculated to be approximately 2.4 in the strain regime below 1.8%, but at higher strains began to increase non-linearly from 4-14. This increased gauge factor is likely caused by mechanical damage to the graphene at larger strain values. It

has been shown previously that as graphene becomes damaged or cracked this leads to an exponential increase in resistance with strain, instead of the expected linear response.[119]

4. Strain Engineering of other Two-Dimensional Crystals

Due to the rapid increase in graphene research other similar materials are gaining increased attention. In particular TMDs have attracted recent interest due to similarities with graphene but with the added benefit of being intrinsic semiconductors with direct band gaps. In particular molybdenum disulphide (MoS_2) has been the focus of many recent investigations which have shown that it is applicable for high efficiency transistors[120] and optoelectronic devices.[121] As with graphene, mechanical strain of these 2D materials leads to a shift in phonon frequency which can be detected by Raman spectroscopy and arises from a change in the electronic structure of the layered material. This strain engineering allows the tuning of the band gap, a shift from a direct to an indirect band gap, and altering of the photonic properties of TMD layered materials.[35,55-57]

The change in electronic structure of monolayer MoS_2 as a function of strain has been calculated theoretically using density functional theory (DFT), and is shown in Figs. 10a and 10b.[35] The downshift in optical absorption, shown in Fig. 10a, is a result of the reduced optical band gap with increasing strain. This could lead to the production of high efficiency photovoltaics or other optoelectronic devices that require sensitivity to specific wavelengths of light. The corresponding band structure of the strained monolayer MoS_2 is shown in Fig. 10b, and shows the reduced optical band gap at the K point with increasing strain as well as the transition from a direct to indirect gap at strain higher strain. This band gap transition has been theoretically predicted by other groups as well and recently observed experimentally as a decrease in photoluminescent intensity.[54,55] Figure 10c shows the schematic of an experimental apparatus to measure the Raman and photoluminescence (PL) spectra of strained monolayer MoS_2.[55] In this example monolayer MoS_2 was mechanically exfoliated and transferred onto a polycarbonate substrate and uniaxial strain was applied by bending the substrate with a four point apparatus. The value of strain

can then be calculated from the radius of the bent substrate, to minimise slippage and increase its adhesion titanium clamps were evaporated onto the MoS_2. Figure 10d plots the Raman spectra of the A′ mode (403 cm^{-1}) due to out-of-plane vibrations along with the E′ mode (384 cm^{-1}) due to in-plane vibrations.[55] Under increasing strain the A′ band shows no noticeable shift in frequency or intensity, while the E′ band splits into two separate peaks (E′$^+$ and E′′) with reduced intensity in a similar fashion as has been observed in graphene. Figure 10e plots the shift in the position of the E′$^+$ and E′′ bands as a function of strain, and both exhibit a linear dependency on strain. The slope of each peak shift is calculated to be 1.0 cm^{-1}/% for the E′$^+$ band and 4.5 cm^{-1}/% for the E′′ band matching the calculated values from first principles.[55] For low strain values (<2%) the results were found to be highly reproducible and could be repeated for multiple strain/relax cycles with little hysteresis. A similar trend as seen in the Raman data was observed in the PL spectra as strain was applied, with a linear shift in PL frequency and a decrease in intensity. The shift in frequency is attributed to the decrease of the optical band gap as calculated previously, while the decrease in intensity is attributed to the shift from direct to indirect transition.[55] The use of strain engineering can therefore be used to tune the desired properties from inorganic 2D layered materials such as MoS_2 as well as graphene. The many similarities between graphene and other 2D materials allows for a wide variety of similar properties to be investigated and exploited for use in electronics applications.

Summary and Future Directions

We have shown in this Perspective several recent examples of how strain can be used to alter the properties of graphene and similar 2D layered materials. However, the ability to tune the properties of layered materials through applied mechanical strain, although proposed theoretically, has yet to be fully realised experimentally. It has been demonstrated that strain can alter the electronic structure of 2D materials such as graphene and TMDs, and the effect is strongly dependent on the angle of this applied strain as well as the structure of the material itself. For future applications in transparent flexible

electronics fully understanding and exploiting these effects is still required, especially at higher strain values (>5%). There still remain many investigations into how strain can be fully utilised to increase the chemical functionalisation of 2D layered materials and the effect of this on the subsequent electronic and mechanical properties. Possible future applications of this strain engineering include hydrogen storage, as the graphene provides a gas storage substrate that can bind and release hydrogen with applied strain reversibly as needed. Electronic devices are another key area, as the increased functionalisation of graphene can lead to the formation of band gap necessary for efficient transistor devices. Different 2D layered materials can also be combined into vertical heterostructures whose properties can then be altered through strain engineering, opening up a wide variety of possibly designs and applications.[59,60,121] Strain engineering of the properties of graphene and other 2D layered crystals is still a relatively new field with many possible routes for further investigations and optimisation to fully realize their potential.

[‡]Current address: Faculty of Engineering and Physical Sciences, School of Chemistry, University of Manchester, UK

References

1.   K. S. Novoselov, A. K. Geim, S. V. Morozov, D. Jiang, Y. Zhang, S. V. Dubonos, I. V. Grigorieva and A. A. Firsov, *Science*, 2004, **306**, 666-669.

2.   A. K. Geim and K. S. Novoselov, *Nat. Mater.*, 2007, **6**, 183-191.

3.   S.-K. Lee, H. Y. Jang, S. Jang, E. Choi, B. H. Hong, J. Lee, S. Park and J.-H. Ahn, *Nano Lett.*, 2012, **12**, 3472-3476.

4.   C. Lee, X. Wei, J. W. Kysar and J. Hone, *Science*, 2008, **321**, 385-388.

5.   R. R. Nair, P. Blake, A. N. Grigorenko, K. S. Novoselov, T. J. Booth, T. Stauber, N. M. R. Peres and A. K. Geim, *Science*, 2008, **320**, 1308.

6.   S. Bae, H. Kim, Y. Lee, X. Xu, J.-S. Park, Y. Zheng, J. Balakrishnan, T. Lei, H. Ri Kim, Y. I. Song, Y.-J. Kim, K. S. Kim, B. Ozyilmaz, J.-H. Ahn, B. H. Hong and S. Iijima, *Nat. Nanotechnol.*, 2010, **5**, 574-578.

7.   Z. Sun, D. K. James and J. M. Tour, *J. Phys. Chem. Lett.*, 2011, **2**, 2425-2432.

8.   K. P. Loh, Q. Bao, P. K. Ang and J. Yang, *J. Mater. Chem.*, 2010, **20**, 2277-2289.

9.   S. Niyogi, E. Bekyarova, J. Hong, S. Khizroev, C. Berger, W. de Heer and R. C. Haddon, *J. Phys. Chem. Lett.*, 2011, **2**, 2487-2498.

10.   C.-C. Lu, Y.-C. Lin, C.-H. Yeh, J.-C. Huang and P.-W. Chiu, *ACS Nano*, 2012, **6**, 4469-4474.

11.   K. S. Kim, Y. Zhao, H. Jang, S. Y. Lee, J. M. Kim, K. S. Kim, J.-H. Ahn, P. Kim, J.-Y. Choi and B. H. Hong, *Nature*, 2009, **457**, 706-710.

12.   B. J. Kim, H. Jang, S.-K. Lee, B. H. Hong, J.-H. Ahn and J. H. Cho, *Nano Lett.*, 2010, **10**, 3464-3466.

13.   S.-K. Lee, B. J. Kim, H. Jang, S. C. Yoon, C. Lee, B. H. Hong, J. A. Rogers, J. H. Cho and J.-H. Ahn, *Nano Lett.*, 2011, **11**, 4642-4646.

14.   P. Avouris, *Nano Lett.*, 2010, **10**, 4285-4294.

15.   F. Bonaccorso, Z. Sun, T. Hasan and A. C. Ferrari, *Nat. Phot.*, 2010, **4**, 611-622.

16.   Y.-M. Lin, C. Dimitrakopoulos, K. A. Jenkins, D. B. Farmer, H.-Y. Chiu, A. Grill and P. Avouris, *Science*, 2010, **327**, 662.

17.   F. Schwierz, *Nat. Nanotechnol.*, 2010, **5**, 487-496.

18.   K. A. Ritter and J. W. Lyding, *Nat. Mater.*, 2009, **8**, 235-242.

19.   K. Todd, H.-T. Chou, S. Amasha and D. Goldhaber-Gordon, *Nano Lett.*, 2008, **9**, 416-421.

20.   Y. Zhang, T.-T. Tang, C. Girit, Z. Hao, M. C. Martin, A. Zettl, M. F. Crommie, Y. R. Shen and F. Wang, *Nature*, 2009, **459**, 820-823.

21.   T. Ohta, A. Bostwick, T. Seyller, K. Horn and E. Rotenberg, *Science*, 2006, **313**, 951-954.

22.   C.-J. Shih, Q. H. Wang, Z. Jin, G. L. C. Paulus, D. Blankschtein, P. Jarillo-Herrero and M. S. Strano, *Nano Lett.*, 2013, **13**, 809-817.

23.   Y. Shi, K. K. Kim, A. Reina, M. Hofmann, L.-J. Li and J. Kong, *ACS Nano*, 2010, **4**, 2689-2694.

24.   S. Niyogi, E. Bekyarova, M. E. Itkis, H. Zhang, K. Shepperd, J. Hicks, M. Sprinkle, C. Berger, C. N. Lau, W. A. deHeer, E. H. Conrad and R. C. Haddon, *Nano Lett.*, 2010, **10**, 4061-4066.

25.   V. M. Pereira and A. H. Castro Neto, *Phys. Rev. Lett.*, 2009, **103**, 046801.

26.   F. Guinea, M. I. Katsnelson and A. K. Geim, *Nat. Phys.*, 2010, **6**, 30-33.

27.   M. Huang, H. Yan, T. F. Heinz and J. Hone, *Nano Lett.*, 2010, **10**, 4074-4079.

28.   N. Levy, S. A. Burke, K. L. Meaker, M. Panlasigui, A. Zettl, F. Guinea, A. H. C. Neto and M. F. Crommie, *Science*, 2010, **329**, 544-547.

29.   G. Cocco, E. Cadelano and L. Colombo, *Phys. Rev. B*, 2010, **81**, 241412.

30.   S.-M. Choi, S.-H. Jhi and Y.-W. Son, *Phys. Rev. B*, 2010, **81**, 081407.

31.   V. M. Pereira, A. H. Castro Neto and N. M. R. Peres, *Phys. Rev. B*, 2009, **80**, 045401.

32.   L. Gong, I. A. Kinloch, R. J. Young, I. Riaz, R. Jalil and K. S. Novoselov, *Adv. Mater.*, 2010, **22**, 2694-2697.

33.   I. Srivastava, R. J. Mehta, Z.-Z. Yu, L. Schadler and N. Koratkar, *Appl. Phys. Lett.*, 2011, **98**, 063102-063103.

34.   R. J. Young, L. Gong, I. A. Kinloch, I. Riaz, R. Jalil and K. S. Novoselov, *ACS Nano*, 2011, **5**, 3079-3084.

35.   J. Feng, X. Qian, C.-W. Huang and J. Li, *Nat. Phot.*, 2012, **6**, 866-872.

36.   J.-H. Wong, B.-R. Wu and M.-F. Lin, *J. Phys. Chem. C*, 2012, **116**, 8271-8277.

37.   C. Attaccalite, L. Wirtz, M. Lazzeri, F. Mauri and A. Rubio, *Nano Lett.*, 2010, **10**, 1172-1176.

38.   X. Dong, D. Fu, W. Fang, Y. Shi, P. Chen and L.-J. Li, *Small*, 2009, **5**, 1422-1426.

39.   D. B. Farmer, R. Golizadeh-Mojarad, V. Perebeinos, Y.-M. Lin, G. S. Tulevski, J. C. Tsang and P. Avouris, *Nano Lett.*, 2008, **9**, 388-392.

40.   S. Park, D. Srivastava and K. Cho, *Nano Lett.*, 2003, **3**, 1273-1277.

41.   R. C. Haddon, *J. Am. Chem. Soc.*, 1986, **108**, 2837-2842.

42.   R. C. Haddon, *Science*, 1993, **261**, 1545-1550.

43.   C. K. Chua and M. Pumera, *Chem. Soc. Rev.*, 2013, **42**, 3222-3233.

44.   F. M. Koehler and W. J. Stark, *Acc. Chem. Res.*, 2013, **46**, 2297-2306.

45.   G. L. C. Paulus, Q. H. Wang and M. S. Strano, *Acc. Chem. Res.*, 2013, **46**, 160-170.

46.   G. Eda and M. Chhowalla, *Nano Lett.*, 2009, **9**, 814-818.

47.   S.-H. Bae, Y. Lee, B. K. Sharma, H.-J. Lee, J.-H. Kim and J.-H. Ahn, *Carbon*, 2013, **51**, 236-242.

48.   Y.-H. Lee and Y.-J. Kim, *Appl. Phys. Lett.*, 2012, **101**, 083102.

49. Y. Wang, R. Yang, Z. Shi, L. Zhang, D. Shi, E. Wang and G. Zhang, *ACS Nano*, 2011, **5**, 3645-3650.

50. M. Huang, T. A. Pascal, H. Kim, W. A. Goddard and J. R. Greer, *Nano Lett.*, 2011, **11**, 1241-1246.

51. Y. Lee, S. Bae, H. Jang, S. Jang, S.-E. Zhu, S. H. Sim, Y. I. Song, B. H. Hong and J.-H. Ahn, *Nano Lett.*, 2010, **10**, 490-493.

52. Q. H. Wang, K. Kalantar-Zadeh, A. Kis, J. N. Coleman and M. S. Strano, *Nat. Nanotechnol.*, 2012, **7**, 699-712.

53. D. Voiry, H. Yamaguchi, J. Li, R. Silva, D. C. B. Alves, T. Fujita, M. Chen, T. Asefa, V. B. Shenoy, G. Eda and M. Chhowalla, *Nat. Mater.*, 2013, **12**, 850-855.

54. P. Lu, X. Wu, W. Guo and X. C. Zeng, *Phys. Chem. Chem. Phys*, 2012, **14**, 13035-13040.

55. H. J. Conley, B. Wang, J. I. Ziegler, R. F. Haglund, S. T. Pantelides and K. I. Bolotin, *Nano Lett.*, 2013, **13**, 3626–3630.

56. K. He, C. Poole, K. F. Mak and J. Shan, *Nano Lett.*, 2013, **13**, 2931-2936.

57. Y. Y. Hui, X. Liu, W. Jie, N. Y. Chan, J. Hao, Y.-T. Hsu, L.-J. Li, W. Guo and S. P. Lau, *ACS Nano*, 2013, **7**, 7126-7131.

58. A. Rimola and M. Sodupe, *Phys. Chem. Chem. Phys*, 2013, **15**, 13190-13198.

59. G.-H. Lee, Y.-J. Yu, X. Cui, N. Petrone, C.-H. Lee, M. S. Choi, D.-Y. Lee, C. Lee, W. J. Yoo, K. Watanabe, T. Taniguchi, C. Nuckolls, P. Kim and J. Hone, *ACS Nano*, 2013, **7**, 7931-7936.

60. A. K. Geim and I. V. Grigorieva, *Nature*, 2013, **499**, 419-425.

61. M. A. Pimenta, G. Dresselhaus, M. S. Dresselhaus, L. G. Cancado, A. Jorio and R. Saito, *Phys. Chem. Chem. Phys*, 2007, **9**, 1276-1290.

62. A. C. Ferrari and D. M. Basko, *Nat. Nanotechnol.*, 2013, **8**, 235-246.

63. A. C. Ferrari, J. C. Meyer, V. Scardaci, C. Casiraghi, M. Lazzeri, F. Mauri, S. Piscanec, D. Jiang, K. S. Novoselov, S. Roth and A. K. Geim, *Phys. Rev. Lett.*, 2006, **97**, 187401.

64. A. Gupta, G. Chen, P. Joshi, S. Tadigadapa and Eklund, *Nano Lett.*, 2006, **6**, 2667-2673.

65. M. M. Lucchese, F. Stavale, E. H. M. Ferreira, C. Vilani, M. V. O. Moutinho, R. B. Capaz, C. A. Achete and A. Jorio, *Carbon*, 2010, **48**, 1592-1597.

66. L. G. Canc□ado, A. Jorio, E. H. M. Ferreira, F. Stavale, C. A. Achete, R. B. Capaz, M. V. O. Moutinho, A. Lombardo, T. S. Kulmala and A. C. Ferrari, *Nano Lett.*, 2011, **11**, 3190-3196.

67. M. Lazzeri and F. Mauri, *Phys. Rev. Lett.*, 2006, **97**, 266407.

68. S. Pisana, M. Lazzeri, C. Casiraghi, K. S. Novoselov, A. K. Geim, A. C. Ferrari and F. Mauri, *Nat. Mater.*, 2007, **6**, 198-201.

69.   A. Das, S. Pisana, B. Chakraborty, S. Piscanec, S. K. Saha, U. V. Waghmare, K. S. Novoselov, H. R. Krishnamurthy, A. K. Geim, A. C. Ferrari and A. K. Sood, *Nat. Nanotechnol.*, 2008, **3**, 210-215.

70.   M. Kalbac, A. Reina-Cecco, H. Farhat, J. Kong, L. Kavan and M. S. Dresselhaus, *ACS Nano*, 2010, **4**, 6055-6063.

71.   T. M. G. Mohiuddin, A. Lombardo, R. R. Nair, A. Bonetti, G. Savini, R. Jalil, N. Bonini, D. M. Basko, C. Galiotis, N. Marzari, K. S. Novoselov, A. K. Geim and A. C. Ferrari, *Phys. Rev. B*, 2009, **79**, 205433.

72.   O. Frank, M. Mohr, J. Maultzsch, C. Thomsen, I. Riaz, R. Jalil, K. S. Novoselov, G. Tsoukleri, J. Parthenios, K. Papagelis, L. Kavan and C. Galiotis, *ACS Nano*, 2011, **5**, 2231-2239.

73.   J. Zabel, R. R. Nair, A. Ott, T. Georgiou, A. K. Geim, K. S. Novoselov and C. Casiraghi, *Nano Lett.*, 2011, **12**, 617-621.

74.   Y. C. Cheng, Z. Y. Zhu, G. S. Huang and U. Schwingenschlögl, *Phys. Rev. B*, 2011, **83**, 115449.

75.   F. Ding, H. Ji, Y. Chen, A. Herklotz, K. Do□rr, Y. Mei, A. Rastelli and O. G. Schmidt, *Nano Lett.*, 2010, **10**, 3453-3458.

76.   M. A. Bissett, W. Izumida, R. Saito and H. Ago, *ACS Nano*, 2012, **6**, 10229-10238.

77.   O. Frank, G. Tsoukleri, I. Riaz, K. Papagelis, J. Parthenios, A. C. Ferrari, A. K. Geim, K. S. Novoselov and C. Galiotis, *Nat. Commun.*, 2011, **2**, 255.

78.   S. Jegal, Y. Hao, D. Yoon, R. S. Ruoff, H. Yun, S. W. Lee and H. Cheong, *Chem. Phys. Lett.*, 2013, **568–569**, 146-150.

79.   O. Frank, G. Tsoukleri, J. Parthenios, K. Papagelis, I. Riaz, R. Jalil, K. S. Novoselov and C. Galiotis, *ACS Nano*, 2010, **4**, 3131-3138.

80.   D. Yoon, Y.-W. Son and H. Cheong, *Phys. Rev. Lett.*, 2011, **106**, 155502.

81.   S. Berciaud, X. Li, H. Htoon, L. E. Brus, S. K. Doorn and T. F. Heinz, *Nano Lett.*, 2013, **13**, 3517-3523.

82.   M. Mohr, J. Maultzsch and C. Thomsen, *Phys. Rev. B*, 2010, **82**, 201409.

83.   M. Mohr, K. Papagelis, J. Maultzsch and C. Thomsen, *Phys. Rev. B*, 2009, **80**, 205410.

84.   M. A. Bissett, M. Tsuji and H. Ago, *J. Phys. Chem. C*, 2013, **117**, 3152-3159.

85.   K. Min and N. R. Aluru, *Appl. Phys. Lett.*, 2011, **98**, 013113.

86.   P. Y. Huang, C. S. Ruiz-Vargas, A. M. van der Zande, W. S. Whitney, M. P. Levendorf, J. W. Kevek, S. Garg, J. S. Alden, C. J. Hustedt, Y. Zhu, J. Park, P. L. McEuen and D. A. Muller, *Nature*, 2011, **469**, 389-392.

87.   A. W. Tsen, L. Brown, R. W. Havener and J. Park, *Acc. Chem. Res.*, 2013, **46**, 2286-2296.

88. G.-H. Lee, R. C. Cooper, S. J. An, S. Lee, A. van der Zande, N. Petrone, A. G. Hammerberg, C. Lee, B. Crawford, W. Oliver, J. W. Kysar and J. Hone, *Science*, 2013, **340**, 1073-1076.

89. J. Zhang, J. Zhao and J. Lu, *ACS Nano*, 2012, **6**, 2704-2711.

90. Y. Wei, J. Wu, H. Yin, X. Shi, R. Yang and M. Dresselhaus, *Nat. Mater.*, 2012, **11**, 759-763.

91. R. Grantab, V. B. Shenoy and R. S. Ruoff, *Science*, 2010, **330**, 946-948.

92. J. Zhang and J. Zhao, *Carbon*, 2013, **55**, 151-159.

93. D. Van Tuan, J. Kotakoski, T. Louvet, F. Ortmann, J. C. Meyer and S. Roche, *Nano Lett.*, 2013, **13**, 1730–1735.

94. Z. Fei, A. S. Rodin, W. Gannett, S. Dai, W. Regan, M. Wagner, M. K. Liu, A. S. McLeod, G. Dominguez, M. Thiemens, A. H. Castro Neto, F. Keilmann, A. Zettl, R. Hillenbrand, M. M. Fogler and D. N. Basov, *Nat. Nanotechnol.*, 2013, **8**, 821-825.

95. J. Lahiri, Y. Lin, P. Bozkurt, I. I. Oleynik and M. Batzill, *Nat. Nanotechnol.*, 2010, **5**, 326-329.

96. J. Kotakoski and J. C. Meyer, *Phys. Rev. B*, 2012, **85**, 195447.

97. F. Hao and D. Fang, *Phys. Lett. A*, 2012, **376**, 1942-1947.

98. N. Chandra, S. Namilae and C. Shet, *Phys. Rev. B*, 2004, **69**, 094101.

99. Y.-I. Jhon, P. S. Chung, R. Smith, K. S. Min, G. Yeom and M. S. Jhon, *RSC Adv.*, 2013, **3**, 9897-9903.

100. T.-H. Liu, G. Gajewski, C.-W. Pao and C.-C. Chang, *Carbon*, 2011, **49**, 2306-2317.

101. H. I. Rasool, C. Ophus, W. S. Klug, A. Zettl and J. K. Gimzewski, *Nat. Commun.*, 2013, **4**, 2811.

102. P. A. Denis and F. Iribarne, *J. Phys. Chem. C*, 2013, **117**, 19048-19055.

103. R. Sharma, J. H. Baik, C. J. Perera and M. S. Strano, *Nano Lett.*, 2010, **10**, 398-405.

104. D.-e. Jiang, B. G. Sumpter and S. Dai, *J. Phys. Chem. B*, 2006, **110**, 23628-23632.

105. C. Tan, J. Rodríguez-López, J. J. Parks, N. L. Ritzert, D. C. Ralph and H. D. Abruña, *ACS Nano*, 2012, **6**, 3070-3079.

106. P. L. d. Andres and J. A. Verges, *Appl. Phys. Lett.*, 2008, **93**, 171915.

107. K. Xue and Z. Xu, *Appl. Phys. Lett.*, 2010, **96**, 063103.

108. V. J. Surya, K. Iyakutti, H. Mizuseki and Y. Kawazoe, *Comput. Mater. Sci.*, 2012, **65**, 144-148.

109. G. Kim, Y. Kawazoe and K.-R. Lee, *J. Phys. Chem. Lett.*, 2012, **3**, 1989-1996.

110. O. Cretu, A. V. Krasheninnikov, J. A. Rodríguez-Manzo, L. Sun, R. M. Nieminen and F. Banhart, *Phys. Rev. Lett.*, 2010, **105**, 196102.

111. D. W. Boukhvalov and Y.-W. Son, *ChemPhysChem*, 2012, **13**, 1463-1469.

112. D. W. Boukhvalov, *RSC Adv.*, 2013, **3**, 7150-7159.

113. A. Udupa and A. Martini, *Carbon*, 2011, **49**, 3571-3578.

114. Q. Wu, Y. Wu, Y. Hao, J. Geng, M. Charlton, S. Chen, Y. Ren, H. Ji, H. Li, D. W. Boukhvalov, R. D. Piner, C. W. Bielawski and R. S. Ruoff, *Chem. Commun.*, 2013, **49**, 677-679.

115. H. Zhang, E. Bekyarova, J.-W. Huang, Z. Zhao, W. Bao, F. Wang, R. C. Haddon and C. N. Lau, *Nano Lett.*, 2011, **11**, 4047-4051.

116. M. A. Bissett, S. Konabe, S. Okada, M. Tsuji and H. Ago, *ACS Nano*, 2013, **7**, 10335-10343.

117. L. Gong, R. J. Young, I. A. Kinloch, I. Riaz, R. Jalil and K. S. Novoselov, *ACS Nano*, 2012, **6**, 2086-2095.

118. X.-W. Fu, Z.-M. Liao, J.-X. Zhou, Y.-B. Zhou, H.-C. Wu, R. Zhang, G. Jing, J. Xu, X. Wu, W. Guo and D. Yu, *Appl. Phys. Lett.*, 2011, **99**, 213107.

119. X. Li, R. Zhang, W. Yu, K. Wang, J. Wei, D. Wu, A. Cao, Z. Li, Y. Cheng, Q. Zheng, R. S. Ruoff and H. Zhu, *Sci. Rep.*, 2012, **2**, 870.

120. B. Radisavljevic, A. Radenovic, J. Brivio, V. Giacometti and A. Kis, *Nat. Nanotechnol.*, 2011, **6**, 147-150.

121. G. Eda and S. A. Maier, *ACS Nano*, 2013, **7**, 5660-5665.

Figures
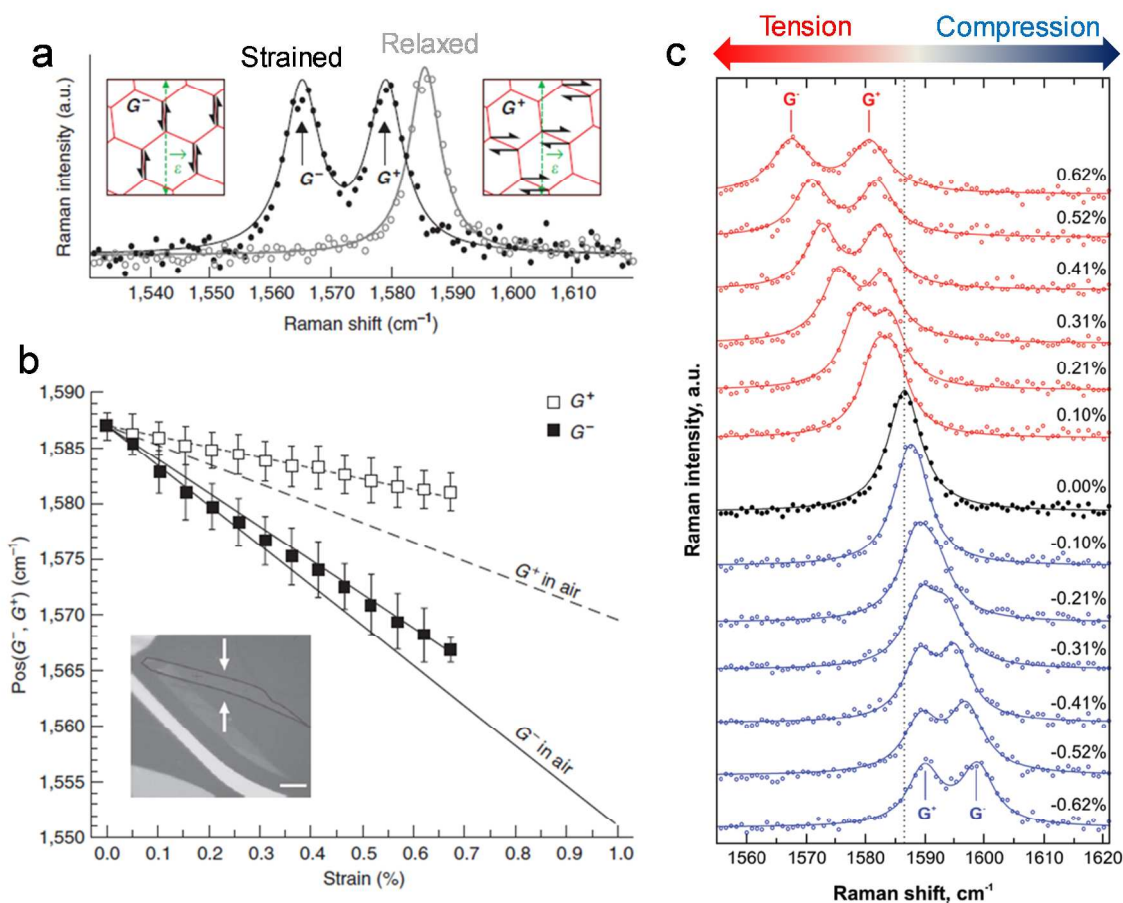
Fig. 1: a) Raman spectrum showing the G band of relaxed graphene (grey) and strained (1%) graphene (black). Inset shows the origin of the G$^+$ and G$^-$ peaks with relation to strain axis (ε). b) Plot of G$^+$ (empty squares) and G$^-$ (filled squares) frequency with increasing uniaxial tensile strain for graphene embedded in polymer depicting linear relationship of each component. Solid lines represent calculated values for suspended graphene. Inset shows an optical photograph of a graphene flake with 10 µm scale bar. Figs. a & b adapted by permission from Macmillan Publishers Ltd: Nature Communications ref.[77], copyright 2011. C) Plot showing the increasing shift and separation of the G band with both tension (red) and compression (blue). Adapted with permission from ref.[79]. Copyright 2010 American Chemical Society.
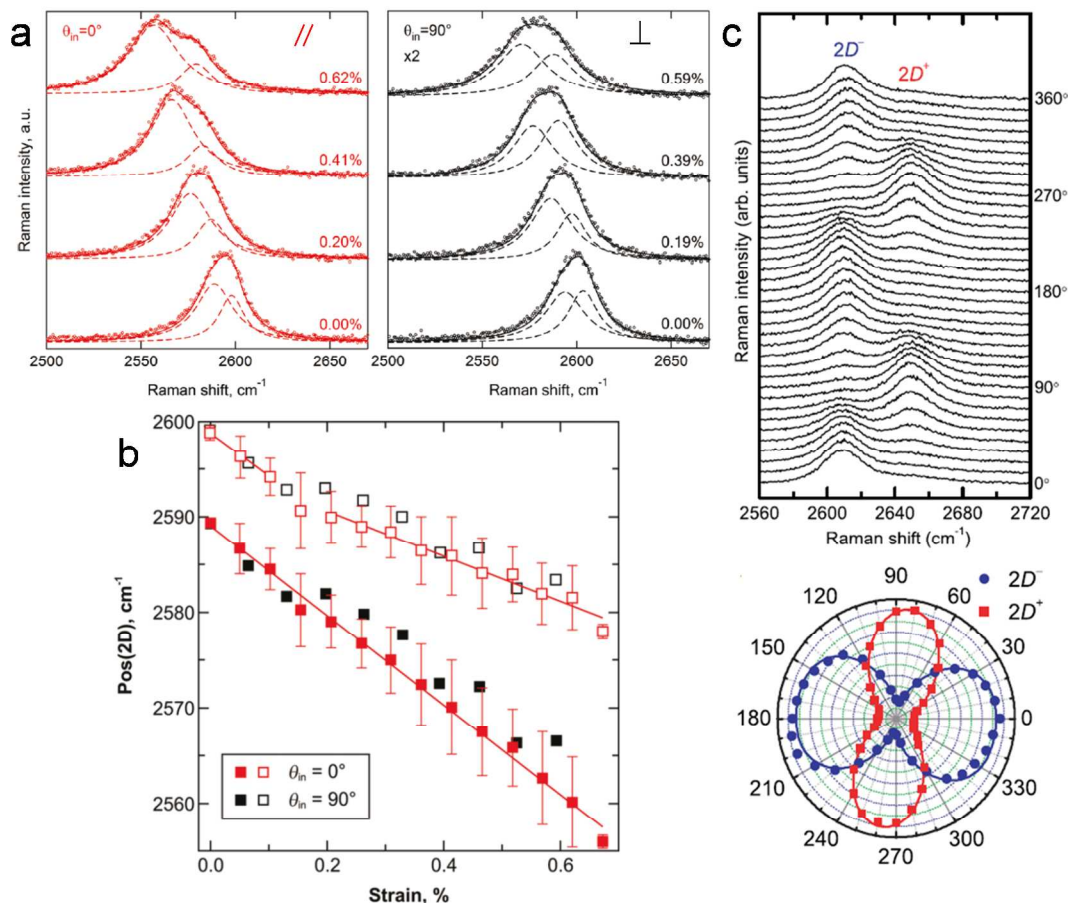
Fig. 2: a) Raman spectra of graphene showing the 2D band with increasing tensile strain applied parallel (red) to the incident excitation polarisation (785 nm) and perpendicular (black). The 2D peak has been fitted with two Lorentzian peaks in each spectrum. **b)** Plot of 2D band frequency with increasing strain depicting linear relationship. The filled and empty squares represent the two individual Lorentzian components for the 2D band line shape and data points corresponding to the perpendicular excitation have been offset by 4 cm^{-1} for clarity. Figs. a & b adapted with permission from ref.[72]. Copyright 2011 American Chemical Society. **c)** Polarised Raman spectroscopy (514.5 nm excitation) of 2D peak with applied tensile strain (0.97%). Top figure depicts the spectra with changing incident polarisation in 10° increments while bottom plots the intensity of each component (2D$^-$, 2D$^+$) in polar coordinates. Adapted from ref.[80]. Copyright 2011 by the American Physical Society.
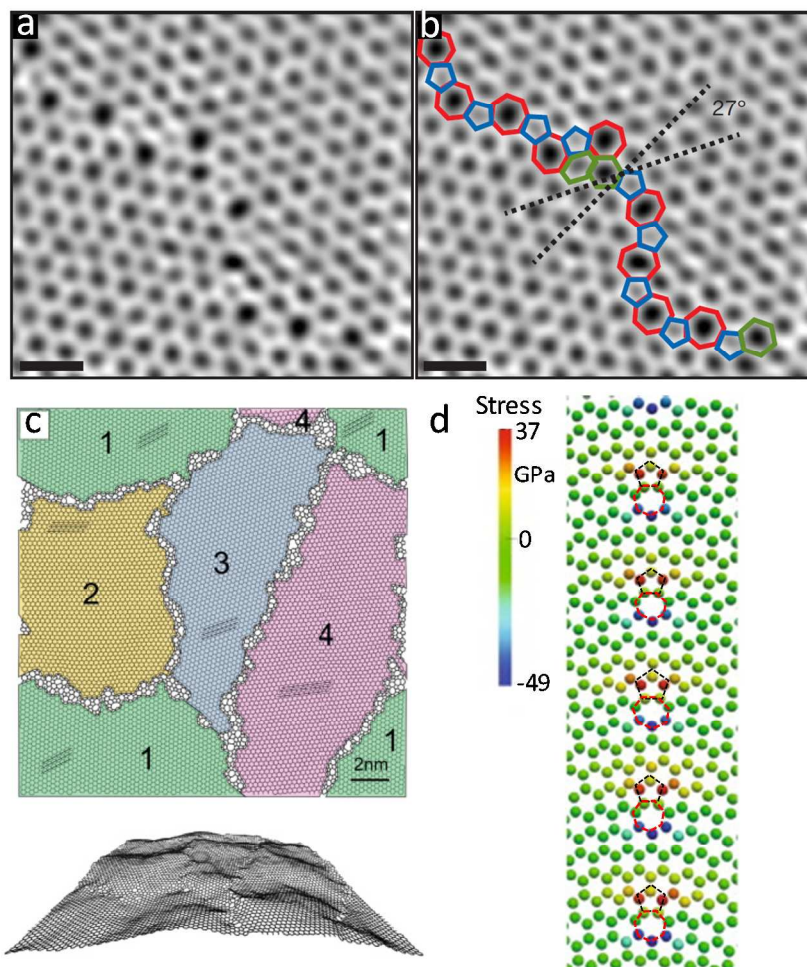
Fig. 3: a-b) Atomic resolution ADF-STEM image showing graphene domain boundary with 5-7 rings highlighted. Scale bars are 5 Å. Figs. a & b adapted by permission from Macmillan Publishers Ltd: Nature ref.[86], copyright 2011. **c)** Atomistic model of polycrystalline graphene showing several rotated domains and domain boundaries (upper) along with crumpled graphene sheet after equilibration (lower). Adapted from ref.[96]. Copyright 2012 by the American Physical Society. **d)** Calculation of inherent strain along domain boundary consisting of 5-7 membered rings, as highlighted. Adapted from ref.[97] with permission from Elsevier.
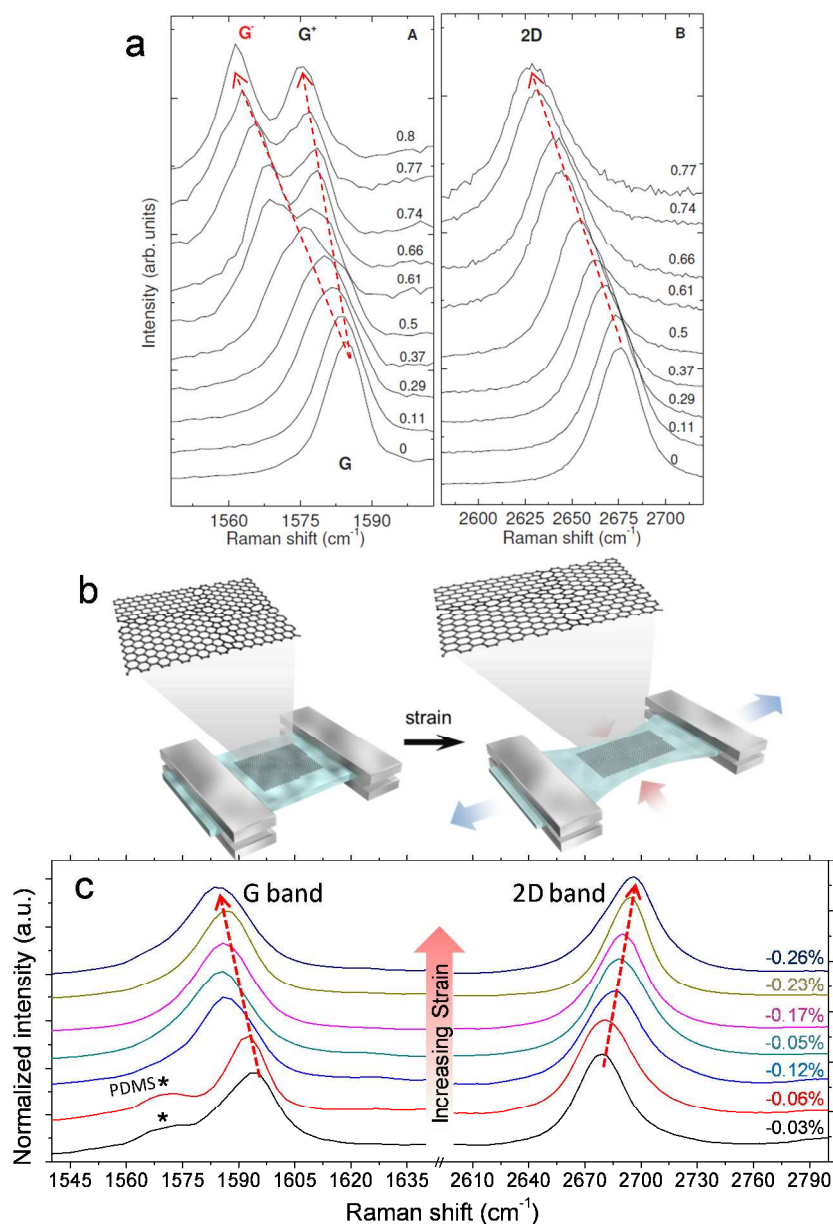
Fig. 4: a) Raman spectra of the G and 2D bands of exfoliated graphene with increasing tensile strain demonstrating the linear trend in the same direction. The numbers indicate the tensile strain ε (%). Adapted from ref.[71]. Copyright 2009 by the American Physical Society. b) Schematic of shear strain applied to polycrystalline graphene supported by a PDMS substrate. c) Raman spectra of polycrystalline graphene as increasing strain is applied showing an opposite trend for the G and 2D bands. The numbers indicate the tensile strain ε (%). Figs. b & c adapted with permission from ref.[76] Copyright 2012 American Chemical Society.
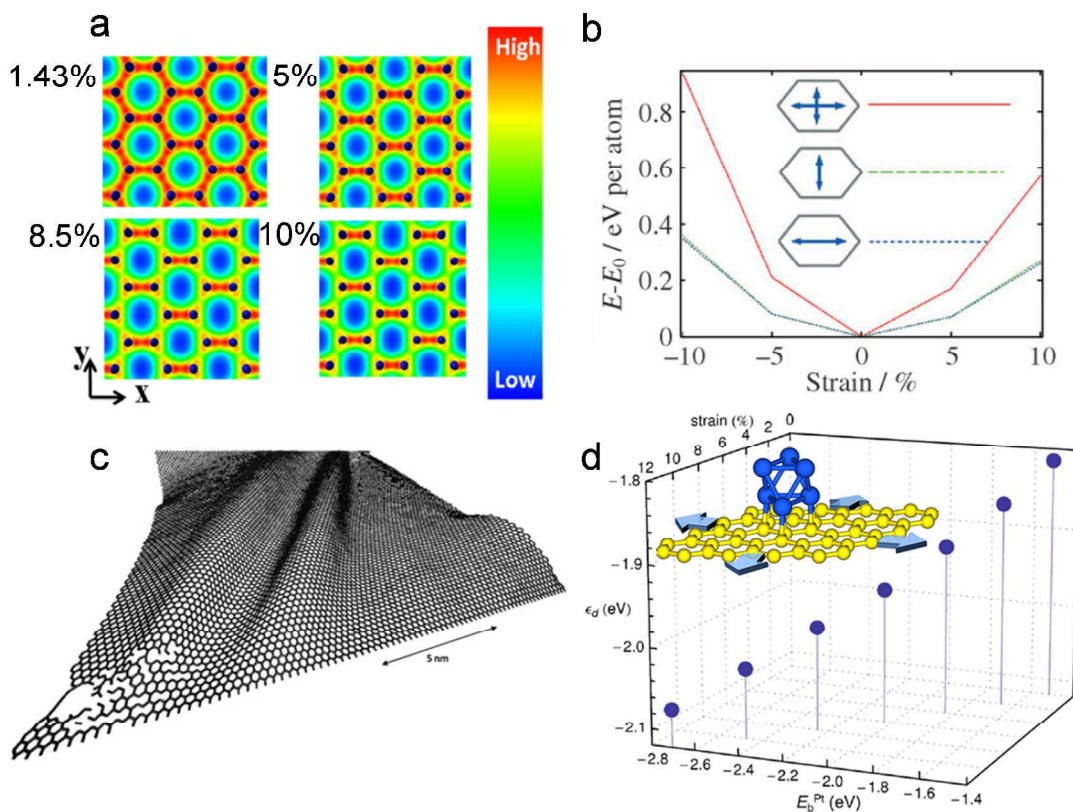
Fig. 5: a) Charge density profile calculated for single-layer graphene under increasing biaxial strain ε (%). Dark blue dots represent C atoms. As strain is increased, electrons become localised around specific C-C bonds. Adapted from ref.[108] with permission from Elsevier. b) Plot of the change in total energy of pristine graphene as a function of strain along the zigzag (blue) and armchair (green) directions as well as biaxial strain (red). Adapted with permission from ref.[111] Copyright 2012 Wiley-VCH. c) Molecular dynamics simulation of single-layer graphene undergoing shear strain, leading to the formation of ridges or ripples in the surface. Adapted from ref.[113] with permission from Elsevier. d) Plot demonstrating the linear correlation between applied strain and the binding energy of platinum clusters on graphene as well as the d-band centre (ϵ_d) of the platinum cluster. The inset schematically demonstrates the biaxial strain applied to the graphene supporting a platinum cluster. Adapted with permission from ref.[109] Copyright 2012 American Chemical Society.
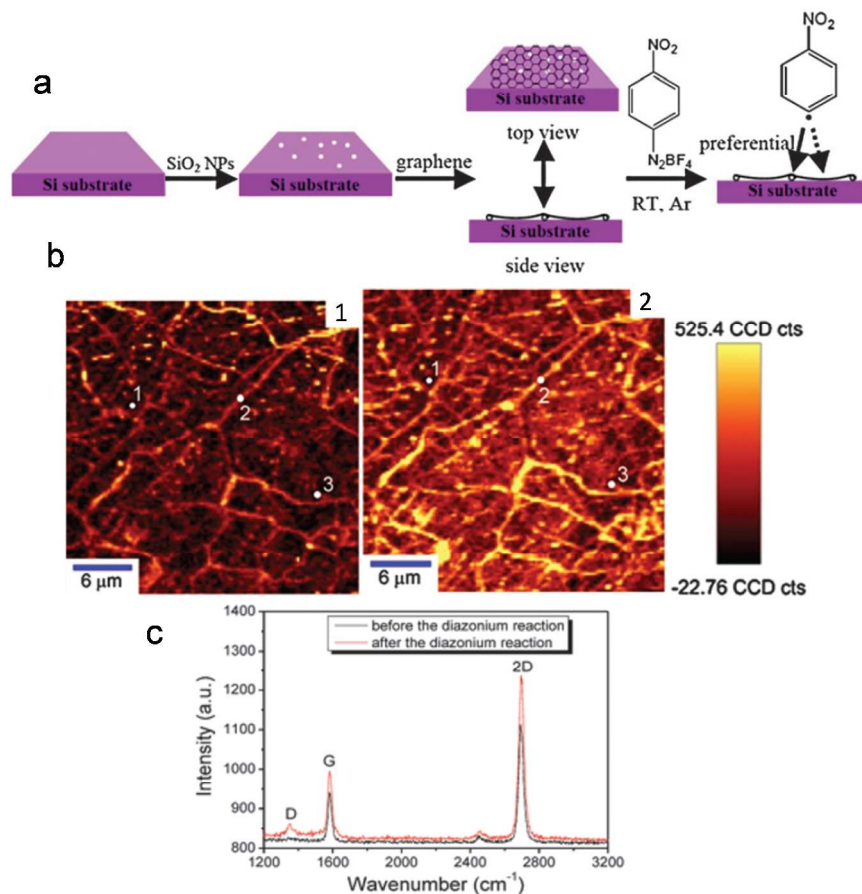
Fig. 6: a) Schematic demonstrating the process of transferring graphene onto silica nanoparticles to create localised strain followed by functionalisation with an aryl diazonium salt (4-nitrobenzene diazonium). b) Raman maps of the D band intensity before (1) and after (2) functionalisation indicating increased functionalisation occurs at strained sites. c) Raman spectra at position marked 3 on the Raman map showing increased D band. Adapted from ref.[114] with permission from The Royal Society of Chemistry.
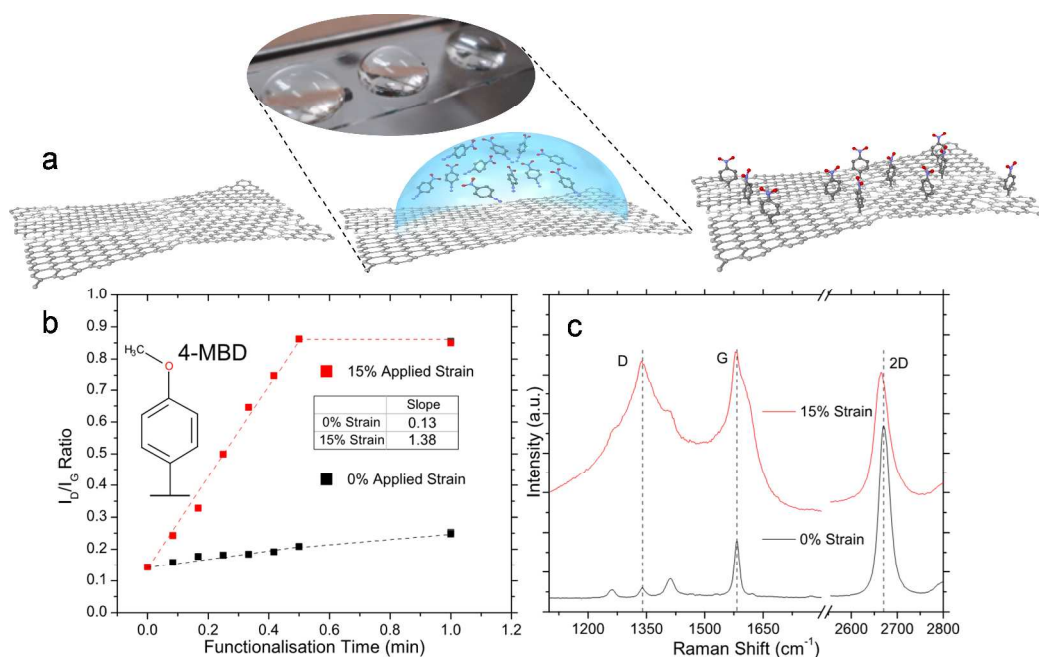
Fig. 7: a) Schematic demonstrating the functionalisation of polycrystalline graphene as shear strain is applied. b) Plot of the I_D/I_G ratio as a function of functionalisation time for one of the studied aryl diazonium compounds 4-MBD (4-methoxybenzene diazonium) without any strain and with 15% applied strain. Note that this 15% strain is applied to the PDMS substrate, and not all the strain is transferred to graphene. c) Comparison of the D, G, and 2D bands of graphene functionalised for 30 seconds with and without applied strain indicating the greatly increased reactivity of the strained graphene. Adapted with permission from ref.[116] Copyright 2013 American Chemical Society.
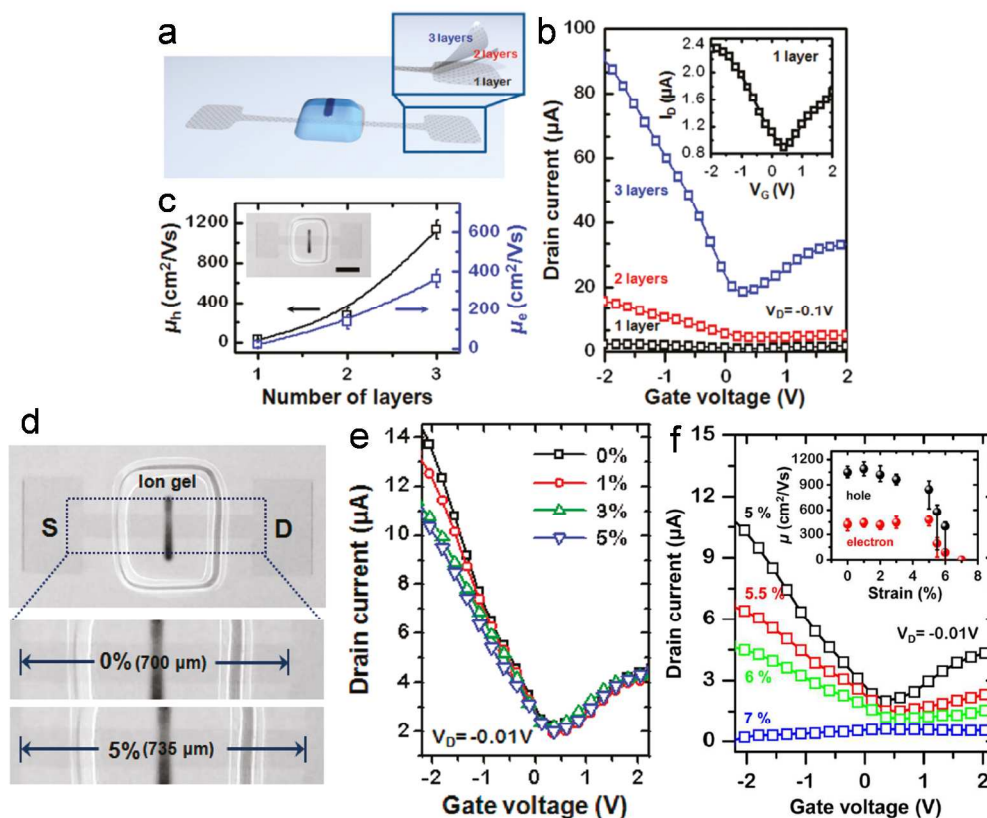
Fig. 8: a) Schematic of a flexible graphene FET on PDMS with ion gel gate dielectric. b) Transfer characteristics for graphene FETs with differing number of graphene layers. c) Plot of hole (μ_h) and electron (μ_e) mobilities with respect to number of graphene layers. Inset shows optical microscope image of tri-layer graphene FET with 300 µm scale bar. d) Optical microscope image of tri-layer graphene FET under 0% and 5% strain. e) I_d-V_G curves for tri-layer graphene FETs with increasing mechanical strain. f) I_d-V_G curves for strain above 5% showing the larger degradation of performance. Inset shows mobility as a function of strain. Adapted with permission from ref.[13] Copyright 2011 American Chemical Society.
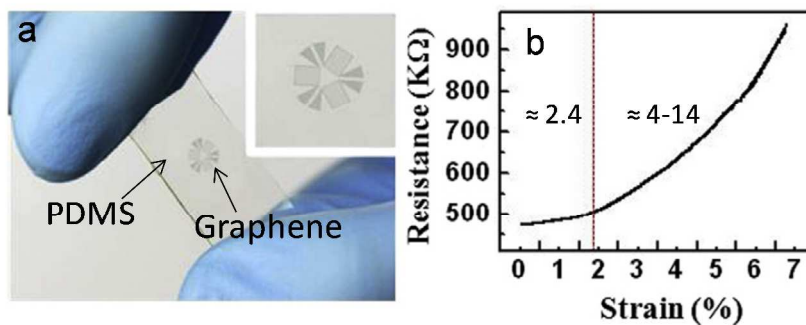
Fig. 9: a) Optical photograph of graphene (≈10 layers) strain sensor in a rosette shape. **b)** Resistance of graphene as tensile strain is applied. The gauge factor is approximately 2.4 below 1.8% then increases non-linearly from 4-14 at higher strain. Adapted from ref.[47] with permission from Elsevier.
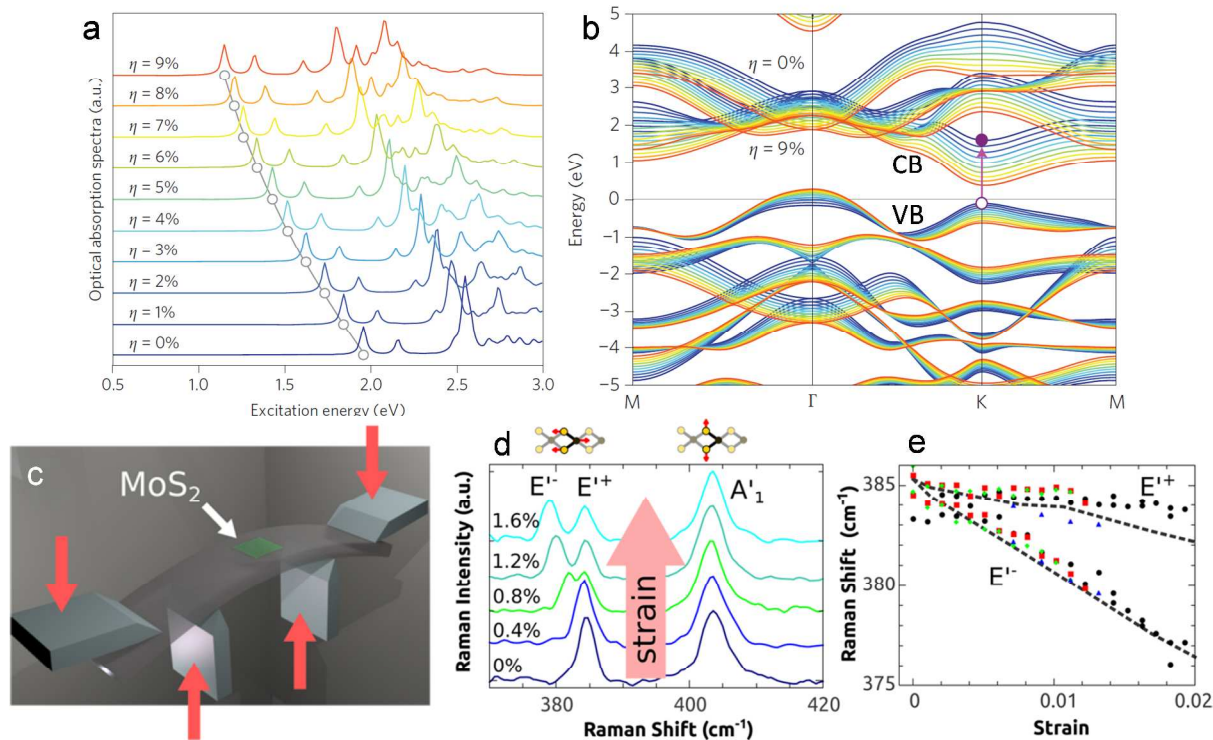
Fig. 10: a) Calculated optical absorption spectra for monolayer MoS$_2$ as a function of bi-axial strain (tension) ranging from 0% to 9%. b) DFT calculated band structure of MoS$_2$ with increasing strain 0-9%. Arrow depicts the minimum direct transition energy for η = 0%. CB and VB are the conduction and valence bands respectively. Figs. a & b adapted by permission from Macmillan Publishers Ltd: Nature Photonics ref.[35], copyright 2012. c) Schematic of experimental apparatus used to strain MoS$_2$ on a polycarbonate substrate. d) Evolution of Raman spectra for strained single-layer MoS$_2$ ranging from 0% to 1.6%. e) Relationship of the Raman E´$^+$ and E´$^-$ bands of single-layer MoS$_2$ with increasing strain. Each colour represents a different device and the dashed lines are from first principles calculation. Figs. (c-e) adapted with permission from ref.[55] Copyright 2013 American Chemical Society.

TOC Figure & Text
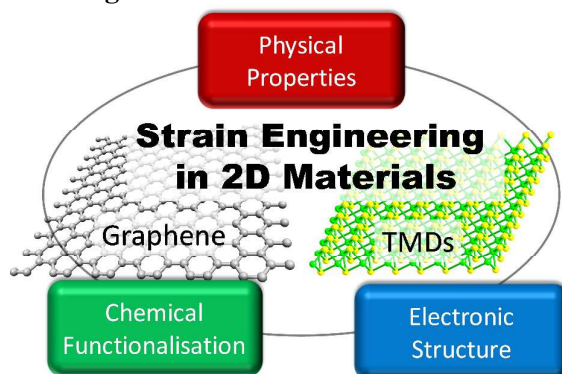
This perspective discusses recent advances in using strain to engineer the properties of thin-layer materials such as graphene and TMDs.